45th AIAA Aerospace Sciences Meeting and Exhibit
8 - 11 January 2007, Reno, Nevada

AIAA 2007-1367

2D CFD simulation of dynamic stall on a vertical axis wind turbine: verification and validation with PIV measurements

Carlos Simão Ferreira* Gerard van Bussel†

Gijs van Kuik‡

Delft University of Technology, Delft, 2629 HS, The Netherlands

After a decrease of interest in the 1990's, the research on Vertical Axis Wind Turbines (VAWT)[a] has reappeared in the last years as a result of the its increasing application in the built environment, where VAWTs present several advantages over Horizontal Axis Wind Turbines (HAWT). The VAWT has an inherent unsteady aerodynamic behavior due to the variation of angle of attack with the angle of rotation θ, perceived velocity and consequentially Reynolds number. The phenomenon of dynamic stall is then an inherent effect of the operation of a Vertical Axis Wind Turbine (VAWT) at low tip speed ratios (λ), having a significant impact in both loads and power.

The complexity of the unsteady aerodynamics of the VAWT makes it extremely attractive to be analyzed using Computational Fluid Dynamics (CFD) models, where an approximation of the continuity and momentum equations of the Navier-Stokes equations set is solved.

The complexity of the problem and the need for new design approaches for VAWT for the built environment has driven the authors of this work to focus the research of CFD modeling of VAWT not in the perspective of creating one large academic model to test a particular situation, but to develop a work that would:

- **verify the sensitivity of the model to its grid refinement (space and time),**
- **evaluate the differences between the different commonly used turbulence models ($Laminar$, $Spalart-Allmaras$ and $k-\epsilon$), and**
- **be evaluated using Particle Image Velocimetry (PIV) experimental data, thus determining the suitability of this data for model validation.**

The 2D model created represents the middle section of a single bladed VAWT with infinite aspect ratio. The model simulates the experimental work[b] of flow field measurement using Particle Image Velocimetry (PIV) by Simão Ferreira et al[1] for a single bladed VAWT, for two different reference Reynolds numbers of $Re = 52000$ and $Re = 70000$ for three tip speed ratios: $\lambda = 2, 3, 4$.

The results show the suitability of the PIV data for the validation of the model, the unsuitability of the application of a single turbulent model and the high sensitivity of the model to grid refinement.

Nomenclature

c	airfoil/blade chord, m
C_N	normal force

*PhD Researcher, Faculty of Aerospace Engineering, Kluyverweg 1, 2629 HS, Delft, The Netherlands.
†Associate Professor, Faculty of Aerospace Engineering, Kluyverweg 1, 2629 HS, Delft, The Netherlands.
‡Professor, Faculty of Aerospace Engineering, Kluyverweg 1, 2629 HS, Delft, The Netherlands.

[a]In this paper the reference VAWT will be used for lift driven VAWT, unless stated otherwise

[b]Note: together with this paper, the authors have submitted to this conference a paper titled "2D PIV visualization of Dynamic stall on a Vertical Axis Wind Turbine", work that precedes the one presented in this paper, describing the experimental work that originated the data used to validate the results of the simulations presented in this paper.

C_T	tangential force
D	rotor diameter, m
k	reduced frequency
R	rotor radius, m
Re	Reynolds number
U_∞	Unperturbed velocity m/s
α	angle of attack
θ	azimuth angle
ω	perturbation frequency
Γ	circulation m^2/s
ρ	density of the fluid kg/m^3
μ_Γ	average value of circulation m^2/s

I. Introduction

The increasing awareness of the need for environmentally sustainable housing and cities has driven the promotion of wind energy conversion systems for the built environment. One of the results of the development of solutions for the built environment is the reappearance of Vertical Axis Wind Turbines (VAWTs). In the built environment, the VAWT presents several advantages over the more common Horizontal Axis Wind Turbines (HAWTs), namely: its low sound emission (consequence of its operation at lower tip speed ratios), better esthetics due to its three-dimensionality (more suitable for integration in some architectural projects, since it follows the sense of volume of the building), its insensitivity to yaw and its increased performance in skewed flow (see Mertens et al[2] and Simão Ferreira et al[3,4]).

The phenomenon of dynamic stall is an inherent effect of the operation of a VAWT at low tip speed ratios (λ). The presence of dynamic stall has a significant impact in both load and power.

Modeling the VAWT in dynamic stall presents five immediate challenges:

- the unsteady component of the flow requires a time accurate model, adding an extra dimension (time) to the numerical grid,
- the geometry of the rotor does not allow for important spatial/time grid simplifications to be applied (example: moving reference frames or radial symmetry),
- the large amount of shed vorticity implies that the model should be sensitive to numerical dissipation and viscous modeling of the vorticity,
- the geometry of a Vertical Axis Wind Turbine results in blade-vortex interaction at the downwind passage of the blade between the blade and the shed vorticity that was generated at the upwind passage. This means that the development of the shed vorticity must be correctly modeled inside the entire rotor diameter; in order to avoid numerical dissipation, the spatial resolution of the grid must be very fine not only in the immediacy of the blades but over the entire rotor, and
- the variation of angle of attack of the blade with azimuth angle implies a varying relation/dominance between lift and drag force on the blade (resulting in moments during the rotation where the VAWT is actually being decelerated because only drag force is present). The correct use of a turbulence model and near-wall models are dominant in these situations. This is particulary important at low tip speed ratios, where the power output of the VAWT is negative (for a certain range of λ); the performance at low tip speed ratios is highly important for start-up behavior, one of the disadvantages usually pointed out to VAWT.

This numerical model aims at simulating the experimental work by Simão Ferreira et al;[1] this experimental work comprises several flow conditions, covering two different Reynolds numbers and three tip sped ratios. Yet, only one Reynolds number ($Re = 50000$) and a single tip speed ratio ($\lambda = 2$) will be considered. Although simulations at other Reynolds numbers and tip speed ratios were performed their presentation in the scope of this paper does not add more insight to the main conclusions.

Contrary to the previous attempts to model the VAWT using CFD (see Hansen et al[5] , Allet et al[6] , Paraschivoiu et al[7] , Paraschivoiu et al[8] and Paraschivoiu[9]), the validation of the results is achieved not by

comparing the load on the blades but by comparing the vorticity in the rotor area. This work aims also at demonstrating the suitability of PIV data for validation of numerical models for this specific problem.

The results of the simulations show the impact of grid refinement and choice of turbulence model. The initial focus of this research (quantification of accuracy) is thus changed into the pursuit of a correct modeling strategy.

II. Model geometry and computational grid

The geometry of the model is a 2D representation of the experimental setup of Simão Ferreira et al.[1] The model's wall boundary conditions consists of two walls spaced $1.25m$, where a $0.4m$ diameter single-bladed Darrieus VAWT is placed. The rotor is represented by an $0.05m$ chord *NACA0015* airfoil and the $0.05m$ rotor axis. The rotor axis is placed over the symmetry position of the wind tunnel. Comparative simulations with and without wind tunnel wall boundary conditions (with and without blockage) showed that there is no significant difference in results and any effect of the wind tunnel walls is negligible. The inlet and outlet boundary conditions are placed respectively $10D$ and $14D$ upwind and downwind of the rotor, allowing a full development of the wake.

The model comprises a 2D spatial grid, simulating the conditions at the middle cross-section of the experimental setup. The grid is composed of four non-conformal sub-grids, each a structured grid of quadrilateral elements. Figure 1 presents a schematic of the shape and location of each sub-grid and the wall boundary conditions representing the airfoil/blade, wind tunnel walls and rotor axis (the flow inlet and outlet boundary conditions are not represented).

The use of sub-grids is necessary due to the movement of the rotor elements. Thus, the sub-grids *Rotor Diameter*, *Blade sub-grid I*, and *Blade sub-grid II* rotate with an angular velocity Ω, while the sub-grid *Wind Tunnel* remains fixed. The option of dividing the rotor space in three sub-grids allows the use of a structured grid without compromising its quality or requiring a large mesh with over refinement in areas of lower importance. A quadrilateral structured grid also allows an easier control of the refinement of the grid; this aspect is crucial in the present work, since the sensitivity to the refinement of the space grid is evaluated.

The most refined sub-grid is *Blade sub-grid I* which defines the geometry of the airfoil and its immediate wake development flow region. The reference fine grid comprises 3305 nodes over the airfoil surface, where the height of the first row of cells is set to $y^+ \approx 1$ (when $\theta = 90°$, $k - \epsilon$ model). The total model size comprises approx. $1.6 * 10^6$ cells.

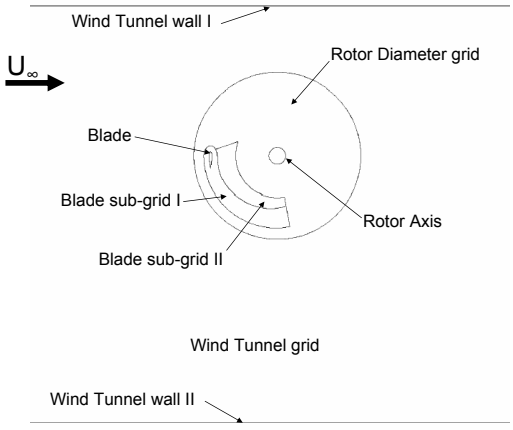

Figure 1. Partial schematic of the model geometry, sub-grid distribution and boundary conditions.

III. Simulated flow conditions

The simulation aimed at representing the flow conditions of the experimental work. Simulations have been performed for $\lambda = 2$, 3, and 4, and incoming flows of $U_\infty = 7.5m/s$ and $10.5m/s$. Yet, for the scope of this paper, only the simulations regarding the case of $\lambda = 2$ and $U_\infty = 7.5m/s$ (resulting in $\Omega = 75rad/s$) are discussed. The level of unsteadiness is determined by the reduced frequency [c] k, which for this experimental work was $k = 0.125$, placing the work in the unsteady aerodynamics region.

Due to the importance of the induction of the rotor, it is necessary to perform a simulation for several rotations until a long fully developed wake is present. All values presented in this paper relate to the revolutions of the rotor after a periodic post-transient solution is found. This transient solution took up to 7 revolutions from the initial stand-still situation to the fully developed wake. This solution was used as a base for the sensitivity analysis; a second transient solution, due to change of grid refinement or turbulence model, took $2-3$ revolutions to overpass.

IV. Verification and validation of *Laminar*, $k-\epsilon$ and $S-A$ models

The limits of the computational hardware and time frame of the computations do not allow the use of a space-time grid fine enough to calculate all scales of turbulence. The use of the different turbulence models, although allowing a coarser grid, impacts the result of the simulation. The increase of computational power in the latest years has lead to the use of increasingly more computationally expensive turbulence models, in the hope of achieving more accurate simulations. Verification of simulation results of an airfoil in a similar Darrieus motion was previously performed by Paraschivoiu[8,9]), with discussion of the differences of results for several one-equation/two-equations Reynolds Averaged turbulence models. Yet, the phenomenon of dynamic stall of the VAWT at low tip speed ratio is highly dependent of the laminar separation occurring at the leading edge. The use of fully turbulent models can limit the occurrence of this laminar separation, resulting in an incorrect turbulent flow development.

This work presents a verification of the effect of applying either a laminar or a turbulent model in the entire flow. The *Laminar* consists of the momentum and continuity equations without closure relations. The $Spalart-Allmaras$ $(S-A)$ and $k-\epsilon$ models assume, respectively, a one-equation and a two-equation model for the eddy viscosity. The description of the models can be found in the Fluent© User's Manual.[10]

Figure 2 shows the values for tangential and normal force over the first 180° degrees of rotation, made non-dimensional by the scale of the airfoil and its rotational velocity ($\frac{1}{2}\rho\lambda^2 U_\infty^2 c$). Notice that the models assuming turbulent flow ($k-\epsilon$ and $S-A$) present similar results, diverging from the laminar model. The normal force C_N [d] -force in the radial direction of the rotor- is, in the laminar case, larger in the first quarter of rotation and lower in the second quarter of rotation, in comparison with the turbulent flow simulations. The laminar flow also presents non-zero normal force at azimuthal angle $\theta = 0$, thus showing an effect on airfoils circulation of the vorticity generated in the downwind portion of the rotation, dragged with the airfoil. A more significant difference is in the tangential component of the force on the airfoil (C_T), which, in the upwind half of the rotation, presents an almost opposite sign of force; the tangential force is very dependent on the friction force, and thus, on the wall treatments associated with each turbulence model. The differences in forces are, despite large, in the range of the difference found in several works where numerical simulations are compared with experimental results of forces or pressure measurements; this result opens some questions regarding the suitability of integral lift force data for the validation of simulations.

The results from the current simulation in terms of flow field measurements are compared with the experimental flow field measurements using PIV of Simão Ferreira et al.[1]Figure 3 shows the phase locked average at $\theta = 96.5°$ of the vorticity field (non-dimensioned by the scale of the airfoil and its rotational velocity) for the three simulations with different turbulence models. Comparing these with the experimental results of the phase locked average vorticity obtained with PIV in the work of Simão Ferreira et al[1] (see figure 4), the *Laminar* model simulation better predicts the development of the large leading edge separated vorticity and the rolling up of the counter-clockwise vorticity at the trailing edge; in fact, the models assuming fully turbulent flow suppress the development of the leading edge separation and present a vorticity

[c] The reduced frequency k is defined as $k = \omega.c/2V$, where ω is the angular frequency of the unsteadiness, c is the blade's chord and V is the velocity of the blade. In this experience, due to the variation of V with rotation angle, k was defined as $k = \omega.c/(2.\lambda.V_\infty) = \omega.c/(2.\omega.R) = c/(2.R)$, where λ is the tip speed ratio and R is the radius of rotation

[d] The normal and tangential forces are presented in their non-dimensioned form C_N and C_T. The scaling is done through the dimensions associated with the airfoil movement $\frac{1}{2}\rho\lambda U_\infty^2 c$.

distribution that does not fit the experimental data. This results shows the unsuitability of using a turbulent model over the entire flow for the simulation of dynamic stall in this Reynolds range.

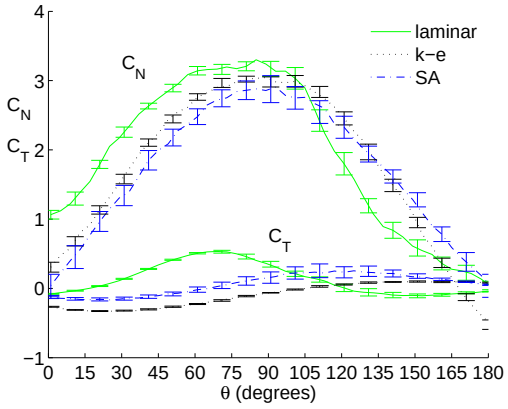

Figure 2. Comparison of normal and tangential force on airfoil calculated with $Laminar$, $k-\epsilon$ and $S-A$ models (first $180°$). The results are the phase locked average over 10 rotations. Error bar represents uncertainty at 95% confidence level.

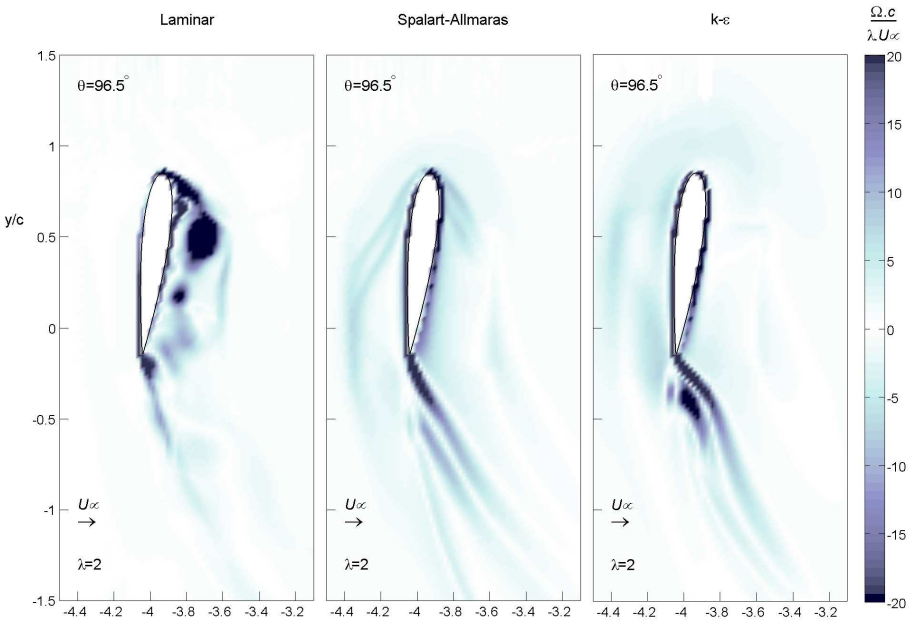

Figure 3. Vorticity field around airfoil for three turbulence model, $\theta = 96.5°$. Each result is the phase locked average of 10 samples.

V. Verification and validation of time grid refinement

On of the most important parameters in a time accurate simulation is the definition of the time step. Figure 5 presents the value of normal and tangential force in the airfoil (first 180°) for four different time steps. The results of normal and tangential force show a significant sensitivity for the refinement of the time grid; the simulations show a divergence between the azimuthal positions of 60° and 160°. This difference can once again be related to the accuracy of the simulation of the development of the leading edge separation vorticity and the consequent development of the trailing edge vorticity roll-up.

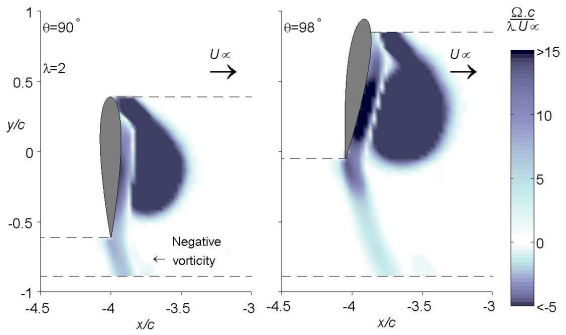

Figure 4. Experimental results of the vorticity (Simão Ferreira et al[1]).

Figure 6 presents the phase locked average of the vorticity around the airfoil for four different time grid refinements at four different positions (in the 90° region). Comparing the simulations with the experimental observations of figure 4 and remaining results of Simão Ferreira et al,[1] it is possible to see that the simulation with $\Delta\ t = 1° * \Omega^{-1}$ presents an underestimation of the generation and evolution of the vorticity, both the one detached at the leading edge and the one shed at the trailing edge. This underestimation is smaller for $\Delta\ t = 0.5° * \Omega^{-1}$ and the simulations with $\Delta\ t = 0.25° * \Omega^{-1}$ and $\Delta\ t = 0.125° * \Omega^{-1}$ present an overestimation of the shed vorticity.

The results show that with increasing refinement of the time grid (Δt), an increasing generation of vorticity at the leading edge occurs, paired by an earlier (in azimuthal position) concentration and rolling up of counter-clockwise vorticity at the trailing edge. This trend can be observed in the value of circulation of the clockwise vorticity shed from the leading edge when compared with the experimental values (figure 7). The value of circulation is calculated in the same procedure as used by Simão Ferreira et al.[1]

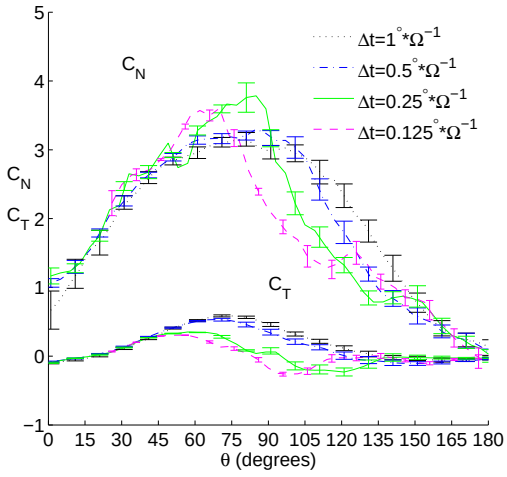

Figure 5. Comparison of normal and tangential force on airfoil with *Laminar* **model, for the cases** $\Delta\ t = 1° * \Omega^{-1}$,$\Delta\ t = 0.5° * \Omega^{-1}$,$\Delta\ t = 0.25° * \Omega^{-1}$ **,and** $\Delta\ t = 0.125° * \Omega^{-1}$ **(first** $180°$**). The results correspond to the phase locked average of** 20, 10, 5 **and** 5 **samples.**

The anticipation/delay of flow phenomena is important to notice. Comparing with experiments, similar vorticity patterns to those observed in the four simulations occur in reality. However, it is the divergence of azimuthal angle at which they occur that is the basis of error of the simulation.

One of the properties of the phenomena of dynamic stall in a Darrieus is the occurrence of a strong random component. Figures 8 and 9 present the phase locked average distributions of vorticity and three instantaneous distributions, for two simulations at different refinements of the time grid. There are two

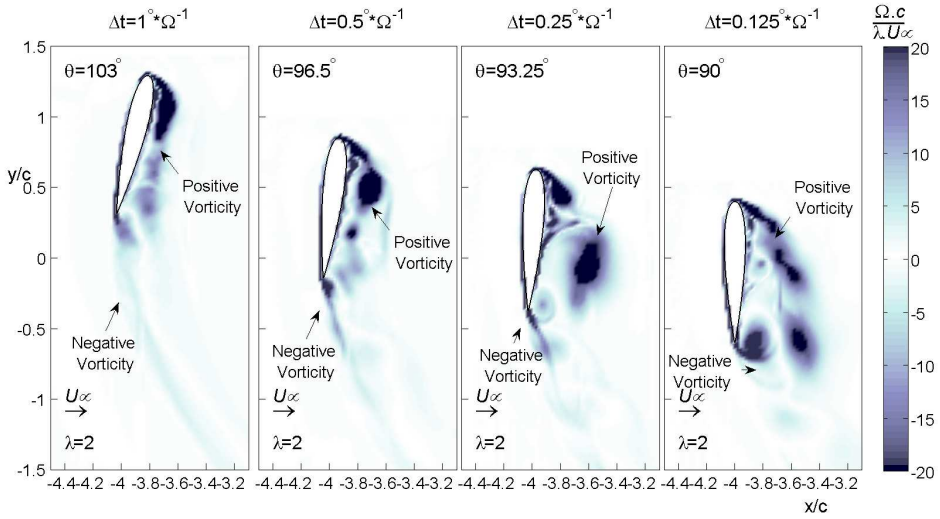

Figure 6. Vorticity field around airfoil for four simulation time steps, after the 90° position (*Laminar* model). The results correspond to the phase locked average of 20, 10, 5 and 5 samples.

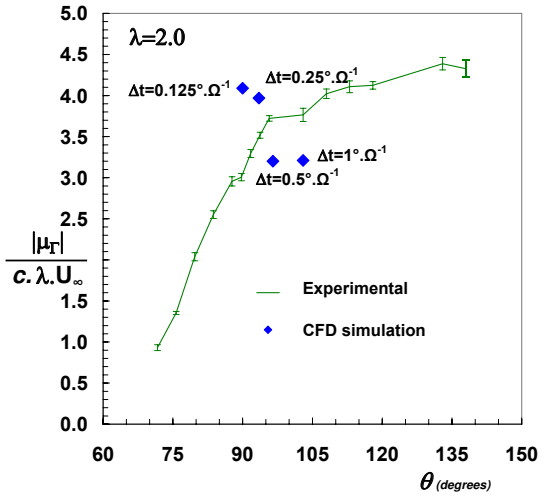

Figure 7. Circulation of the separated leading edge vorticity. Comparison of simulation values with experimental results.

aspects to compare between the two cases: the presence of more and smaller vortices relating to the leading edge separated vorticity in the case of lower refinement, as compared with the presence of only two large clockwise vortices in the case of a more refined time grid; and the larger size of the counter-clockwise vorticity generated over the surface of the airfoil (past the first leading edge vortex) in the finer grid case.

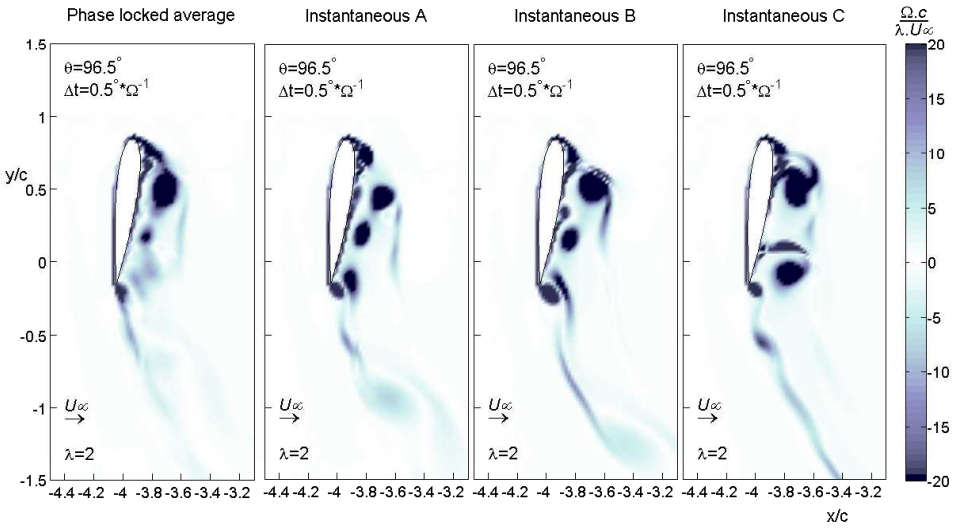

Figure 8. Comparison of phase locked average with instantaneous sample, $\Delta\ t = 0.5° * \Omega^{-1}$, $\theta = 96.5°$.

Comparing the simulations with the phase locked averaged and instantaneous experimental measurements of figures 10 and 11 (neglecting the difference of azimuthal position), it is possible to see that in the coarser time grid there is an over fragmentation/spreading of the vorticity, in the case of the finer time grid, there is a over concentration of vorticity in two single large vortices.

Although the results do not represent accurately all the properties of the real flow, they point to the possibility of the random component having a mainly $2D$ origin and thus, being passible of simulation through a $2D$ model (avoiding the expenses of a $3D$ representation).

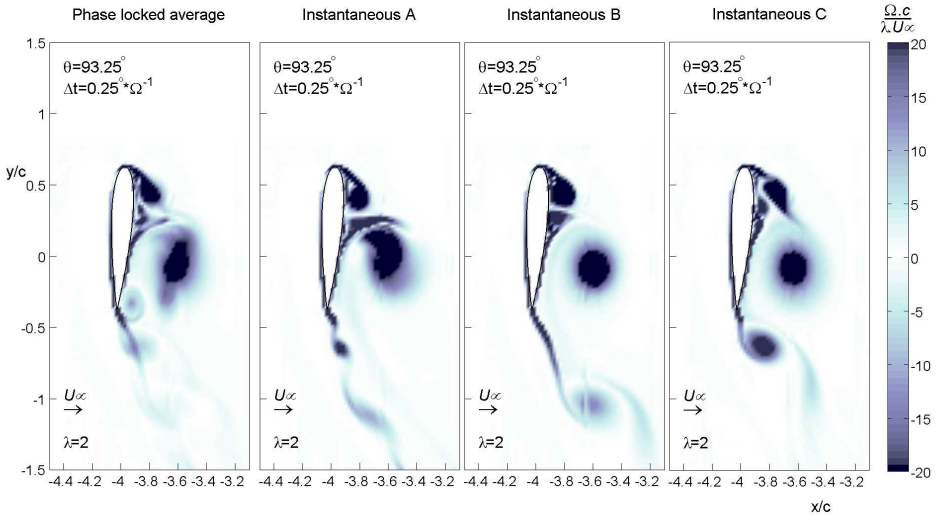

Figure 9. Comparison of phase locked average with instantaneous sample, $\Delta\ t = 0.25° * \Omega^{-1}$, $\theta = 96.5°$.

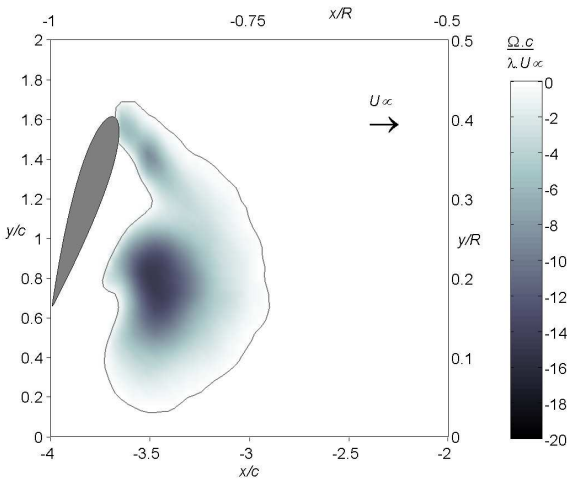

Figure 10. Vorticity field around airfoil (experimental PIV data), phase locked average, $\theta = 113°$.

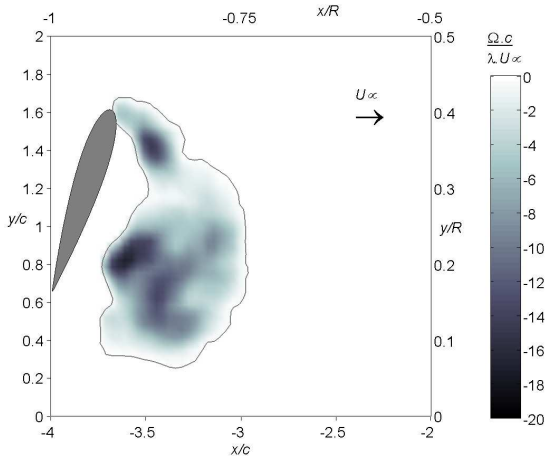

Figure 11. Vorticity field around airfoil (experimental PIV data), instantaneous sample, $\theta = 113°$.

VI. Verification of the influence of spatial grid size

Having verified the influence of the refinement of the grid in time, it is now necessary to view the implication of a coarsening of the spatial grid.

In this section we compare the results of the reference fine grid with a model in which the sub-grid *Blade sub-grid I* is coarsened by a factor of 4 in area (the distance between nodes in x an y are doubled). The comparison for the simulated resulting forces for the reference and coarsened grid is shown in figure 12. The forces for the coarse space grid follow the trend seen in the case of refinement of the time grid. These force development are a result of the characteristics of vorticity development previously observed.

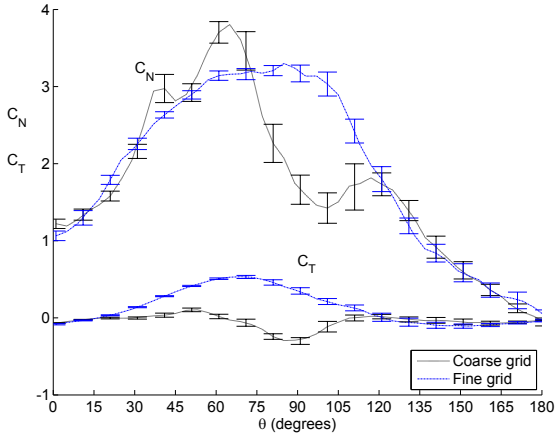

Figure 12. Comparison of normal and tangential force on airfoil , reference fine and coarse grids, $\Delta\, t = 0.5° * \Omega^{-1}$. The results correspond to the phase locked average of 10 samples.

Figure 13 compares the phase locked vorticity distribution of fine and coarse mesh at $\theta = 96.5°$. In the coarsened mesh the over estimation of the leading edge vorticity and early roll-up of the trailing edge vorticity occurs, as previously seen in the case of refinement of the time grid, but in this case in opposite direction.

VII. Conclusions

The results of the CFD simulations indicate the unsuitability of using a single turbulence model scheme for the numerical simulation of a 2D Darrieus in dynamic stall at low tip speed ratios. The use of 1-equation/2-equation models that assume turbulent flow over the entire field results in a partial suppression of the magnitude of the leading edge laminar separation and in a reduction of maximum normal force. Although the resulting flow field of the three turbulent models differ totally in the spatial distribution of vorticity, the average tangential and normal forces over the upwind semi-rotation of the airfoil is similar, thus showing the difficulty of using experimental force/performance data for the validation at low λ. The *Laminar* model, although more suitable for the simulation of the leading edge separation, leads,at increasing refinement of the time grid, to over prediction of the generation and evolution of the vorticity.

The experimental flow field data obtained using Particle Image Velocimetry proved to be a very useful method of validation of the rotor aerodynamics, since it gives direct insight into the the flow behavior (contrary to the total force, which is an integral result of the aerodynamics).

Further research will aim at developing numerical simulations with multiple turbulence models over the grid, thus aiming to improve the simulation of the development of the counter-clockwise vorticity shed at the trailing edge (resulting in a more correct development of the leading edge separation vorticity).

References

[1]Simão Ferreira, C., van Bussel, G., and van Kuik, G., "2D PIV visualization of dynamic stall on a vertical axis wind turbine," *Abstract submited for the 2007 AIAA/ASME Wind Energy Symposium*, 2007.

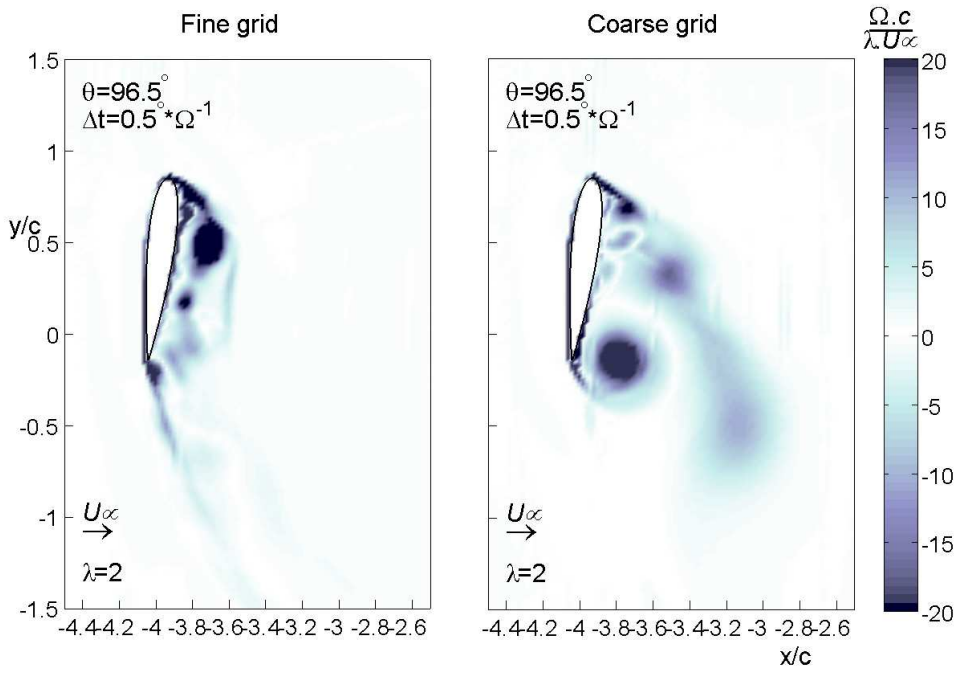

Figure 13. Comparison of the vorticity field around airfoil for coarse and fine grid, $\theta = 96.5°$.

[2]Mertens, S., van Kuik, G., and van Bussel, G., "Performance of a H-Darrieus in the Skewed Flow on a Roof," *Journal of Solar Energy Engineering*, Vol. 125, 2003, pp. 433–440.

[3]Simão Ferreira, C., van Bussel, G., and van Kuik, G., "An analytical method to predict the variation in performance of an H-Darrieus in skewed flow and its experimental validation," *Proceedings of the European Wind Energy Conference 2006*, 2006.

[4]Simão Ferreira, C., van Bussel, G., and van Kuik, G., "Wind tunnel hotwire measurements, flow visualization and thrust measurement of a VAWT in skew," *AIAA/ASME Wind Energy Symposium*, 2006.

[5]Hansen, M. and Søresen, D., "CFD Model for Vertical Axis Wind Turbine," *Wind Energy for the New Millennium-Proceedings of the European Wind Energy Conference, Copenhagen, Denmark*, 2001.

[6]Allet, A., Hallé, S., and Paraschivoiu, I., "Numerical Simulation of Dynamic Stall Around an Airfoil in Darrieus Motion," *Journal of Solar Energy Engineering*, Vol. 121, February 1999, pp. 69–76.

[7]Paraschivoiu, I. and Allet, A., "Aerodynamic Analysis of the Darrieus Wind Turbines Including Dynamic-Stall Effects," *Journal of Propulsion and Power*, Vol. 4, No. 5, 1988, pp. 472–477.

[8]Paraschivoiu, I. and Béguier, C., "Visualization, Measurements and Calculations of Dynamic Stall for a Similar Motion of VAWT," *Proceedings of the European Wind Energy Conference, Herning, Denmark*, 1998.

[9]Paraschivoiu, I., *Wind Turbine Design - With Emphasis on Darrieus Concept*, Polytechnic international Press, 2002.

[10]*Fluent User's Manual*, Fluent Inc.